Monte Carlo Simulations of Bragg Peak Curves for Mono-Energetic Proton Beams

Saleh M. Ben Saleh
Department of Physics and Material Science,
Tajoura Nuclear Research Centre-Libya
saleh.bsaleh@gmail.com
bensalemary@yahoo.com

Hajer M. Albangahzi
Department of Physics and Material Science,
Tajoura Nuclear Research
Centre-Libya
harsbs@yahoo.com

Shrifa M. Alarabi
Department of Physics and Material Science,
Tajoura Nuclear Research Centre-Libya
Reema2783@gmail.com

Abstract— **As an energetic proton beam penetrates into matter its energy loss rate (stopping power) increases with penetration depth reaching a maximum value in a region known as Bragg peak. The main objective of this study is to determine the penetration depths of mono- energetic protons in water using Monte Carlo simulations.. The outputs of the simulations were analysed using ROOT analysis software. Validation of the Monte Carlo model was carried out by comparing proton ranges in water obtained with Geant4 simulations against data obtained from the NIST database. The simulation results were in excellent agreement (within an approximately 0.5% uncertainty) with NIST data.**

Index Terms: **Monte Carlo, Electromagnetic interaction, Nuclear interaction, Proton, GEANT4, Bragg peak, ROOT.**

I. INTRODUCTION

Radiotherapy using proton beams was first suggested by Wilson in 1946 [1]. Unlike photons and electrons, protons have the advantage in radiotherapy because of their depth dose profile (the Bragg peak effect) as well as minimal scattering. Hence protons have the ability to concentrate the dose inside the tumour volume with limited dose exposure to the surrounding healthy tissues. Nowadays, proton beams of intermediate energies (ranging from 60-250 MeV) are widely used for radiotherapy applications. For example, 60-70 MeV proton beams are used for the radiotherapeutic treatment of ocular tumours, whereas 160-250 MeV proton beams are suitable for treating deep seated tumours.

When energetic protons travel through matter, they are subject to electromagnetic and nuclear interactions with the targeted atoms. These interactions are responsible for the energy loss of protons along their penetration depths into an absorber [2]. Evaluation of proton range in a medium can be done either experimentally [3-5] or through Monte Carlo simulation [6-8].

Received 8 Agu 2017; revised 23 Aug 2017; accepted 7 Sept 2017.

Available online 10 Sept 2017.

The Monte Carlo (MC) method provides different physics models to simulate almost all probable interactions of particles with matter. Over the years several MC softwares, including FLUKA [9], MCNPX [4], and GEANT4 [5] have been developed to allow the user to simulate a particular interaction process. The GEANT4 (GEometry ANd Tracking) is a C++ Monte Carlo toolkit [11, 12] that can be used to simulate the radiation transport through matter. It contains various sets of physics models describing the physical interactions for electrons, photons, protons, neutrons and many other particles.

The present study had three objectives: firstly, to simulate the electromagnetic and nuclear interactions of proton (with energies 60, 70, 90, 100, 120, 150, 200 and 250 MeV) in a water phantom using Geant4 Monte Carlo toolkit; secondly, to determine accurately the proton ranges from simulated Bragg peak curves and finally to simulate the energy spectra profiles of secondary particles arising from the proton inelastic nuclear interactions with the target atoms.

II. BRIEF THEORY: PROPERTIES OF PROTONS

The physics of proton energy deposition is the driving force for their use in radiation therapy. When protons penetrate into an absorber (matter), they deposit energy through electromagnetic and nuclear interactions processes with the atoms of the target (absorber). Electromagnetic interactions include inelastic Coulomb interactions with the orbital electrons and elastic Coulomb interactions with the nucleus whereas nuclear interactions consist mostly from inelastic interactions with the nucleus of the materials [2].

The mean energy loss of protons resulted from inelastic Coulomb collisions with atomic electrons of an absorber is described by the Bethe-Bloch equation [13, 14]:

$$-\left\langle \frac{dE}{dx} \right\rangle = \frac{4\pi e^4 Z_0^2}{m_e v^2} Z_1 \left[\ln \frac{2m_e c^2 \beta^2}{I\left(1-\beta^2\right)} - \beta^2 \right] + \left(corrections\right) \quad (1)$$

Where, m_e is the rest mass of the electron, Z_0 and Z_1 are the atomic numbers for the projectile and the target respectively, $\beta = \frac{v}{c}$ (v represents the velocity of the projectile where c is the speed of light in vacuum), and I is the average excitation energy of the target material. In inelastic Coulomb collisions with atomic electrons, proton loses its kinetic energy by mainly the ionization process. For a huge number of collision events with atomic electrons, the energy loss rate is small and occurs in a continuous manner. The Bethe-Bloch equation implements a Continuous Slowing Down Approximation (CSDA) assumption for the calculations of the proton's energy loss. Detailed reviews and derivation of equation (1) can be found in literature [15].

Elastic Coulomb interaction with the target nuclei is the predominant cause of proton scattering [16]. "Figure. 1" illustrates the interaction process of proton colliding with target nuclei. The incident particle experiences repulsive forces from the target nuclei that cause small angle deflections of the proton. This effect is called Multiple Coulomb Scattering (MCS), it is responsible for the lateral spread out of the beam profile. Coulomb scattering distribution is approximately Gaussian [17] for small- angle deviations and is described by the following formula [18, 19]:

$$\theta_0 = \frac{14.1MeV}{pv} z \sqrt{\frac{l}{L_R}\left(1+\frac{1}{9}\log_{10}\frac{l}{L_R}\right)} \qquad (2)$$

Where, p is the momentum of the particle, v is the velocity of the projectile, z is the charge of the projectile. L_R and l are the medium's radiation length and path length respectively. Gottschalk et `al (1993) worked out detailed discussions of multiple Coulomb scattering of proton beams [20].

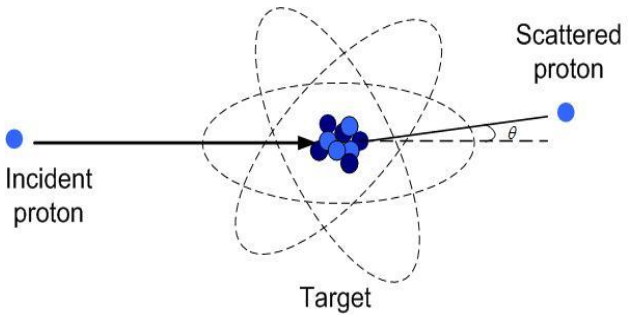

Figure 1. Schematic Representation of Elastic Coulomb Collision of a Proton with the Target Nuclei, Multiple Collisions Cause Small Angle-Deflections of a Proton along its Path.

Furthermore, protons can also undergo inelastic nuclear interactions with the target nucleus. "Figure. 2" is a schematic representation of inelastic nuclear collision of a proton with the target nucleus. Inelastic collisions break up the target nuclei causing the emissions of secondary particles such as secondary protons, neutrons, gamma, alpha particles plus heavy fragments such as deuterons and tritons.

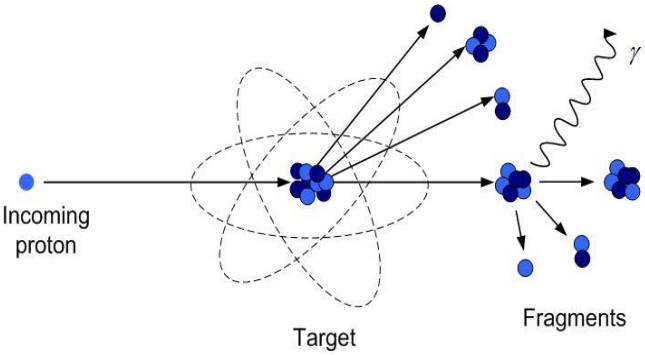

Figure 2. Diagram of an Inelastic Nuclear Collision of a Proton with the Target Nuclei, Resulting in the Break-up of the Target Nucleus with the Emission of Secondary Particles and Heavy Fragments.

The range of proton denoted by $R(E)$, defined as the average distance travelled in a material, with an initial energy E_0 is obtained by integrating the Bethe-Bloch formula (equation 1) reciprocally [21, 22]:

$$R(E) = \int_{E_0}^{0} \left(-\frac{dE}{dx}\right)^{-1} dE \qquad (3)$$

For clarification, two types of logical terminologies of proton range in a material are come across in the literature namely the CSDA range and the projected range. The former accounts only for the inelastic collisions of proton with the atomic electrons, where the latter takes into account the multiple Coulomb scattering as well.

III. MATERIALS AND METHODS

In this study, the Monte Carlo simulations were carried out using Geant4 Toolkit [11] (version 10.p02) running under Linux system. The setup depicted in "Figure. 3" was used for simulation of proton range in water phantom. A cubical water phantom with dimensions of 40 × 30 × 30 cm^3 was modelled. The water phantom was irradiated by a mono-energetic proton beam (with different energies ranging 60, 70, 90, 100, 120, 150, 200 and 250 MeV). The proton source was located at 8 cm distance away from the water phantom. The beam axis was in the x-direction. The space outside the water phantom was vacuum that very low density ($\rho = 10^{-25}$ g/cm^3).

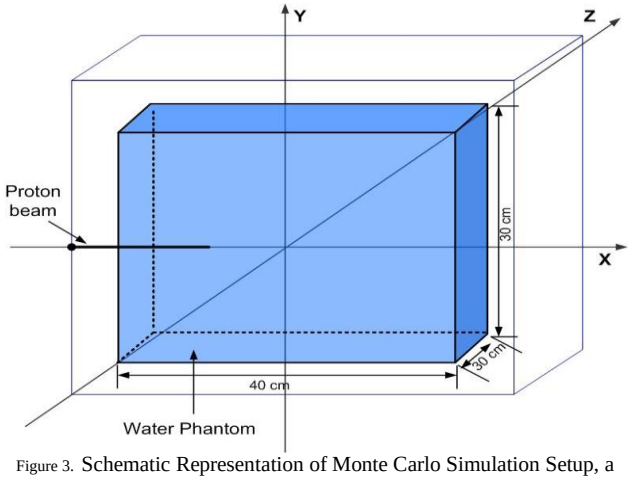

Figure 3. Schematic Representation of Monte Carlo Simulation Setup, a Water Phantom (Dimensions not to Scale) is Irradiated by a Proton Beam Towards the x-axis.

To include the physical interactions of proton with matter, we implemented different set of physics models. Firstly, the Standard Physics Model "EmStandardPhysics-option3" physics list was selected to track the proton beam; it simulates only the electromagnetic interaction processes of protons with the target materials. The CSDA range simulation was performed by turning off the physics option "activate MCS" process. The projected range simulation was carried out by turning on the physics option "activate MCS" process. Secondly, the Binary physics model was chosen to simulate the nuclear inelastic interactions of the primary particle with the target nucleus. Additionally, the QGSP_BIC_HP physics model was selected to determine the energy spectra of the secondary particles arising from the inelastic nuclear interactions with the target nucleus.
The number of histories for each simulation was set to 10^7 particles. The outputs of the simulations were stored into a ROOT [23, 24] files for further analysis. ROOT is data analysis software written in C++ language and developed by the European Centre for Nuclear Research (CERN). We generated ROOT commands for plotting and superimposing simulated data.

IV. RESULTS AND DISCUSSION

The stopping power, which is an average value for the energy loss per unit distance, for protons due to Coulomb interactions with target electrons is summarized in table 1. "Figure. 4&5" represent the stopping power for protons due to Coulomb interactions with electrons. As proton enters the medium, it's stopping power (energy loss) increases firstly at slow rate with depth producing constant ionization density in region known as the plateau region. And then the stopping power for protons increases very sharply near of the particle range, before dropping to almost zero value. This peaking up of stopping power near the end of the particle range is called Bragg peak. As can be seen from "Figure. 6", the stopping power at the Bragg peak position was higher for 60 MeV protons (around 6.6 MeV/mm) than for 250 MeV proton beams (about 2.6 MeV/mm). Lower energy beams have a higher peak-to-plateau stoping power ratio. This is because lower energy beams have narrower Bragg peaks. The width of the Bragg peak increases with energy.

Table 1. The Stopping Powers for Protons due to Coulomb Interactions with Wlectrons (all Ionization Processes were Switched on).

Proton energy (MeV)	Stopping power (MeV/mm) at Bragg peak	Bragg peak location (cm)
60	6.6	3.10
70	6.4	4.09
90	5.4	6.43
100	5	7.80
120	4.4	10.71
150	3.7	15.85
200	3.1	26.08
250	2.6	38.10

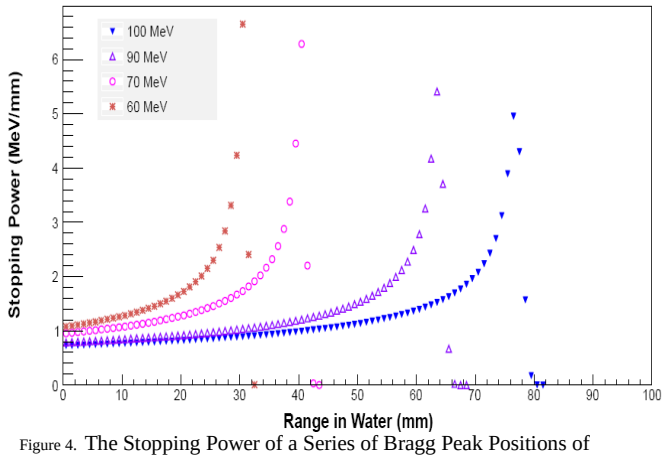

Figure 4. The Stopping Power of a Series of Bragg Peak Positions of Proton Beams with Energies of 60 and 100 MeV.

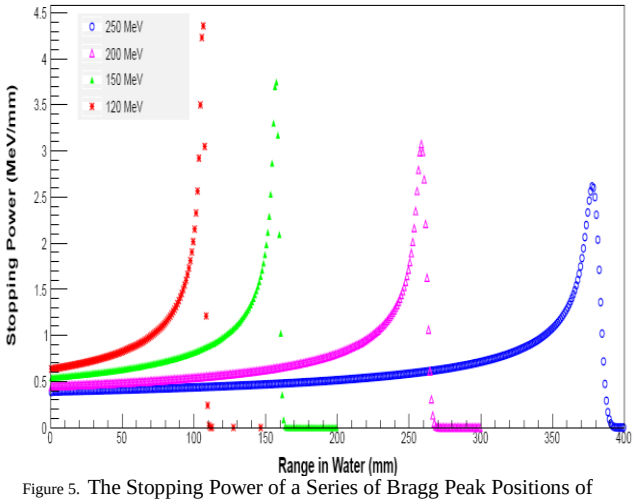

Figure 5. The Stopping Power of a Series of Bragg Peak Positions of Proton Bbeams with Energies of 120 and 250 MeV.

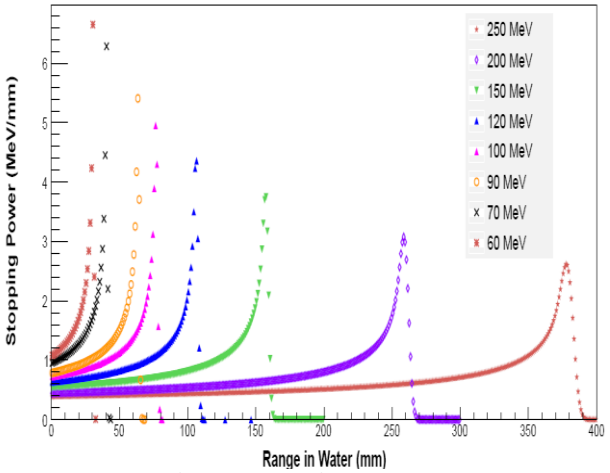

Figure 6. A Series of Bragg Peaks of Proton Beams with Variable Energy Ranges.

Another relevant process is Multiple Coulomb scattering of protons in matter which takes place as a consequence of the interaction with the target nuclei. MCS has consequences both on the lateral width and range straggling of proton beams. The stopping power for protons due to MCS process is shown in table 2. "Figure. 7,8 and 9" represented the stopping power as a function of range in water of the two electromagnetic interactions (ionization and MCS process). MCS had a small effect on the location of Bragg peak for any given energy range.

Table 2. The Stopping Power for Protons due to Coulomb Interactions with Nuclei (Ionization and MCS Processes were Switched on).

Proton energy (MeV)	Stopping power (MeV/mm) at Bragg peak	Bragg peak location (cm)
60	6.4	3.08
100	4.5	7.70
120	4.2	10.62
150	3.5	15.69
200	2.8	25.68
250	2.4	37.25

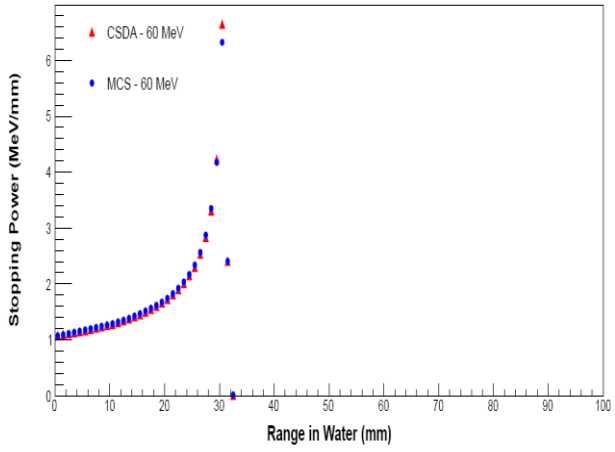

Figure 7. Bragg peak Curves for the Two Components of Electromagnetic Interactions of 60 MeV Proton Beams.

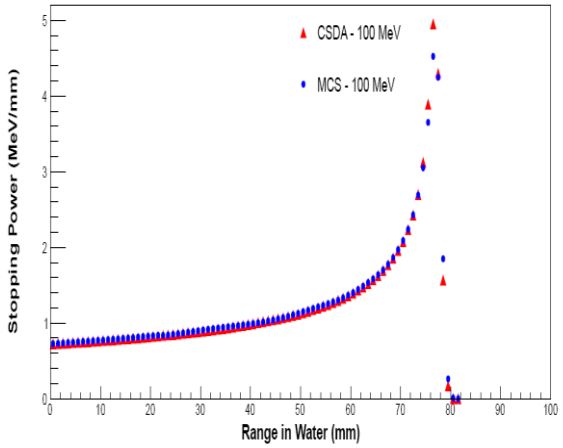

Figure 8. Bragg peak Curves for the Two Components of Electromagnetic Interactions of 100 MeV Proton Beams.

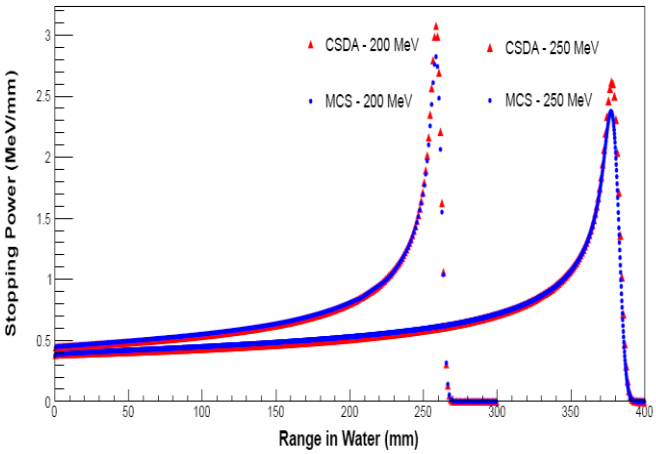

Figure 9. Bragg peak Curves for the Two comp Onents of Electromagnetic Interactions of 200 and 250 MeV Proton Beams.

"Figure. 10&11" illustrate the impact of inelastic nuclear interactions on the Bragg peak curves. Non-elastic nuclear interactions occur mostly in the entrance region of Bragg curve, where the stopping power is generally low and varies only slightly. Nuclear collisions have no effect on the location of the Bragg peak.

Inelastic nuclear interactions produce classes of secondary particles such as secondary protons, neutrons and heavy charged fragments. For proton therapy, secondary protons emerging from the incident proton beam create a halo of dose distributions around the beam and should be taken into account while performing absolute dosimetry [25]. Neutrons may as well contribute an extra (low) dose in the patient that may cause a risk of secondary cancer especially in children and pregnant women [26-28]. The contribution of secondary particles originating from inelastic nuclear interactions with the target nuclei, to the dose distributions in the neighbourhood of the incident beam have not been widely studied. However, we are currently undertaking Monte Carlo simulations to investigate the contribution of secondary particles to the dose distributions on the

basis of a phantom constructed from the Computed Tomography (CT) patient geometry.

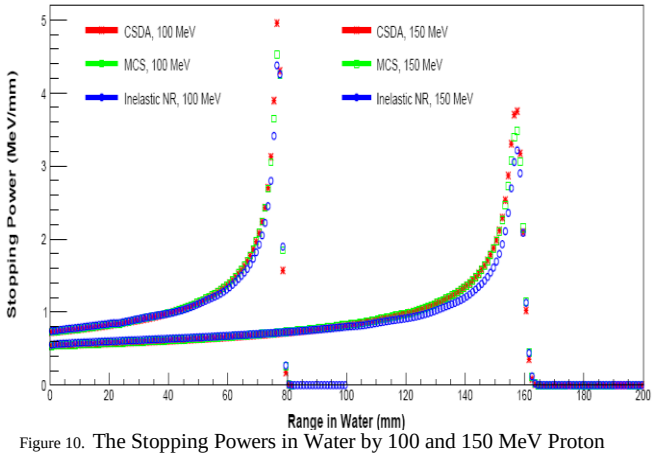

Figure 10. The Stopping Powers in Water by 100 and 150 MeV Proton Beams as a Function of Penetration Depth for the three Components of the Interactions of the Incident Beam.

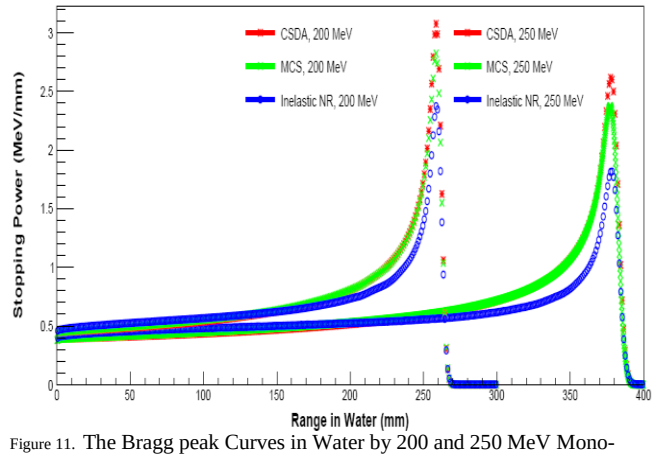

Figure 11. The Bragg peak Curves in Water by 200 and 250 MeV Mono-Energetic Protons for Different Components of Interactions.

"Figure. 12-16" show the energy spectra of the secondary particles yielded from inelastic nuclear interactions with the target nuclei. The yield is defined as the number of fragments (secondary particles) produced per primary projectile. The results were based on simulated protons with variable energy, as indicated in the legend. Gammas, deuterons and alpha spectra produced from these proton beams have relative low mean energies of 3 MeV, 10 MeV and 6 MeV respectively as obtained from the simulation. The neutron spectrum produced from 250 MeV proton beams (see "Figure. 16") have a mean energy of 68 MeV. No neutrons of energies greater than 250 MeV were produced. The spectral information of secondary particles may be used to estimate the contribution of these products to the dose distribution in the neighborhood of the incident proton beams. Some experimental data suggest that secondary particles such as recoils may cause a measurable amount of damage to the tissues adjacent to the target [29].

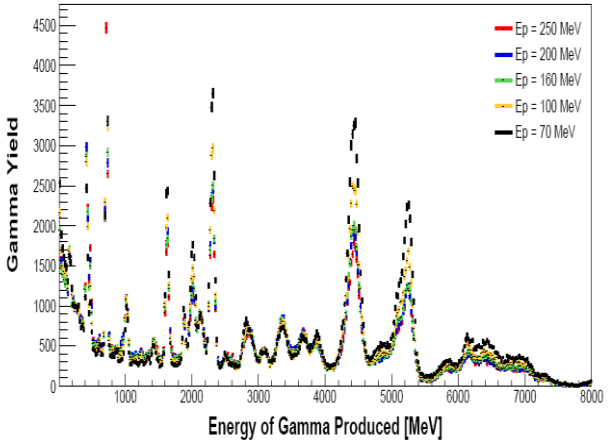

Figure 12. Energy Spectra of Gamma rays Arising from Inelastic Nuclear Interactions of Protons (Energy from 70 to 250 MeV) with the Target Nuclei.

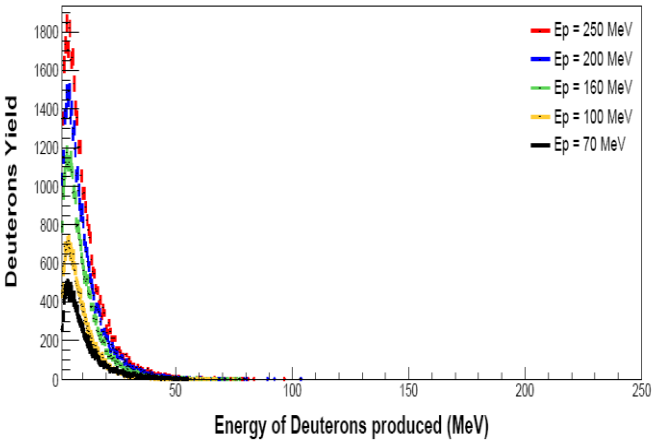

Figure 13. Energy Spectra of Deuterons Arising from Inelastic Nuclear Interactions of Protons (Energy from 70 to 250 MeV) with the Target Nuclei.

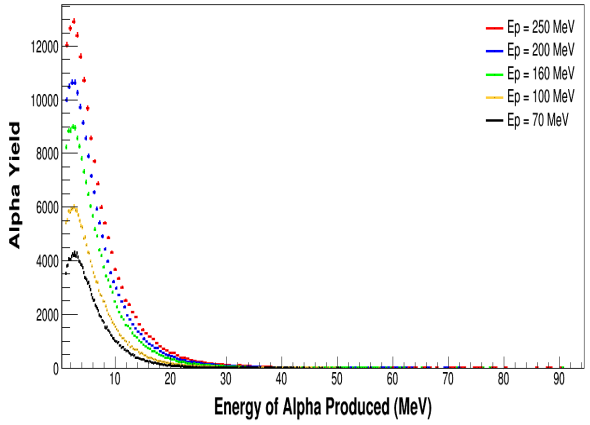

Figure 14. Energy Spectra of Alpha particles Arising from Inelastic Nuclear Interactions of Protons (Energy from 70 to 250 MeV) with the Target Nuclei. The X-axis was Rescaled for Clarification Reason.

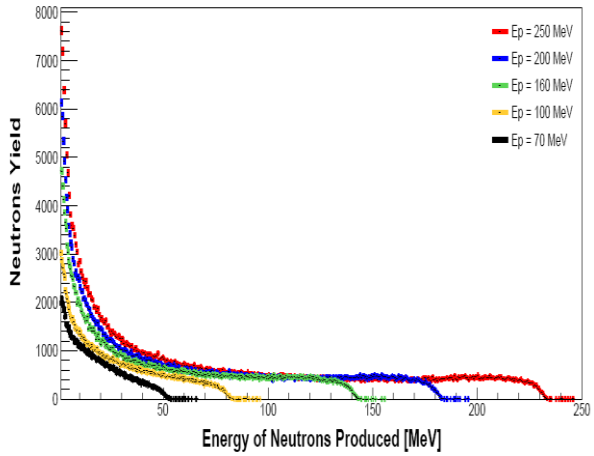

Figure 15. Energy Spectra of Neutrons Arising from Non-Elastic Nuclear Interactions of Protons (Energy from 70 to 250 MeV) with the Target Nuclei.

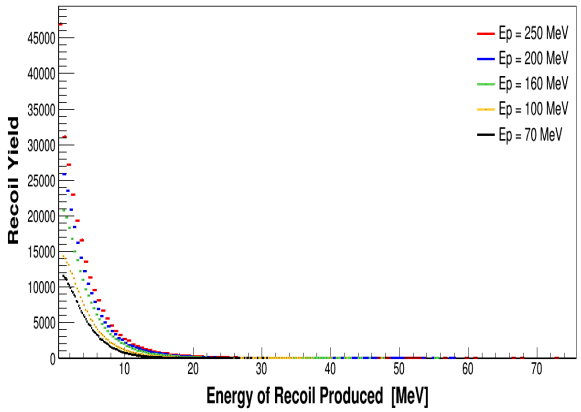

Figure 16. Energy Spectra of Recoil Nuclei Arising from Inelastic Nuclear Interactions of Protons (Energy from 70 to 250 MeV) with the Target Nuclei. The X-axis was Rescaled for Clarification Reason.

Monte Carlo techniques are more extensively used for simulating radiation transport in matter: because of providing reliable and accurate results. However, these results still need to be validated against experimental measurements (where possible) to be trustful.

In CSDA simulations, ranges of proton corresponded to follow primary particle ionization energy loss only. Whilst in projected range simulations, ranges of proton were obtained by switching on the ionization processes and MCS process simultaneously. Table 3 shows the results of the range of mono-energetic proton beams in water. The statistical uncertainty in Monte Carlo data was within 1%. Simulated data were compared against data obtained from the United States National Institute of Standards and Technology (NIST) database [30]. Tables 4 and 5 revealed the similarity between the two distributions. The data were plotted "Fig. 17" and showed an excellent agreement between the two distributions. This demonstrates the accuracy of Monte Carlo simulations.

Table 3. Simulation Results of the CSDA Range of Mono-Energetic Proton Beams in Water.

Energy (MeV)	Range (cm)	Root Mean Square (cm)	Relative error (%)
60	3.10	0.043	1.41
70	4.09	0.057	1.39
90	6.43	0.090	1.40
100	7.75	0.108	1.39
120	10.71	0.146	1.36
150	15.85	0.208	1.31
200	26.07	0.335	1.29
250	38.10	0.482	1.27

Table 4. Comparison between Simulated and NIST Data of the CSDA Range of Proton Beams in Water.

Energy (MeV)	CSDA range (cm) Geant4 Simulation	CSDA range (cm) NIST database	Difference (%)
60	3.106	3.093	0.40
70	4.098	4.080	0.43
90	6.430	6.398	0.50
100	7.758	7.718	0.52
120	10.716	10.660	0.52
150	15.853	15.770	0.53
200	26.079	25.960	0.46
25o	38.101	37.940	0.42

$$\%difference = \frac{|NIST - Simulation|}{NIST} \times 100$$

Table 5. Comparison between Simulated and NIST Data of the Projected Range of Proton beams in Water.

Energy (MeV)	Projected range (cm) Geant4 Simulation	Projected range (cm) NIST database	Difference (%)
60	3.084	3.089	0.14
100	7.701	7.707	0.07
120	10.624	10.665	0.24
150	15.668	15.760	0.46
200	25.683	25.930	0.95
25o	37.253	37.900	1.71

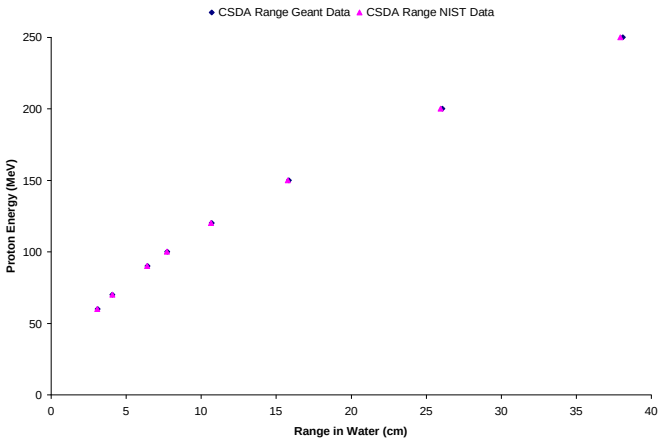

Figure 17. Comparison between Simulated CSDA and NIST Data of the Range of Mono-Energetic Proton Beams in Water. The Relative Statistical Uncertainty of the Monte Carlo Simulation was within 1.4%.

IV. CONCLUSION

The stopping power for protons of different energies in water was investigated by using Geant4 Monte Carlo Toolkit. The simulation considered the electromagnetic and nuclear interactions of mono-energetic proton beams travelling through a cubical water phantom. The simulation produced Bragg peak curves which represented the amount of energy delivered by the incident proton as a function of the depth in the target.

The location of Bragg peak for proton beams is energy dependent. Most of the energy lose of the proton is due to ionization processes. Elastic Coulomb interactions with the nucleus cause small-angle deflections along the proton path. Whilst inelastic nuclear interactions with the nuclei produce secondary particles and heavy fragments. The CSDA and projected ranges for protons were determined from simulated Bragg peak curves and evaluated using ROOT data analysis software. The Monte Carlo results were compared to data obtained from NIST database for proton ranges in water. The two distributions were found to be in excellent agreement. An accurate Monte Carlo model has been constructed; it will be used for further research studies in the field of proton therapy.

ACKNOWLEDGMENTS

The authors wish to thank colleagues Dr. Zakria Aburas and Mr Muhsen Hamedi for useful comments on the manuscript, many thanks also go to TNRC librarian Moufida Alsunni for her technical help.

REFERENCES

1. R. R. Wilson, "*Radiological use of fast protons*". Radiology, 1946, 47:487-491.
2. R. D. Evans, "*The Atomic Nucleus". Mc Graw-Hills (1955).*
3. *K. Parodi, H. Paganetti, H. A. Shih, S. Michaud, J. S. Loeffler, T. F. DeLaney, Liebsch NJ, et al, "Patient study of in vivo verification of beam delivery and range, using positron emission tomography and computed tomography imaging after proton therapy*". Int. J. Radiat. Oncol. Biol. Phys. 2007, 68:920–34.
4. T. Liamsuwan, S. Uehara, D. Emfietzoglou, and H. Nikjoo, "*Physical and biophysical properties of proton tracks of energies 1 keV to 300 MeV in water*". Inter. Jour. Radiat. Biolo. 2011, 87:141–160.
5. A. C. Knopf, K. Parodi, H. Paganetti, T. Bortfeld, J. Daartz, M. Engelsman, N. Liebsch, and H. Shih, "*Accuracy of proton beam range verification using post-treatment positron emission tomography/computed tomography as function of treatment site*". Int J. Radia. Oncolo. Biol. Phys. 2010, 1–8.
6. K. Parodi, A. Mairani, S. Brons, J. Naumann, M. Kramer, F. Sommerer, and T. Haberer, "*The influence of lateral beam profile modifications in scanned proton and carbon ion therapy: a Monte Carlo study*". Phys. Med. Biol. 2010, 55:5169–87.
7. L. Grevillot, D. Bertrand, F. Dessy, N. Freud, and D. Sarrut, "*GATE as a GEANT4-based Monte Carlo platform for the evaluation of proton pencil beam scanning treatment plans*". Phys. Med. Biol. 2012, 57:4223–44.
8. C. C. Lee, J. Y. Lee, J. C. Tung, W. H. Cheng, and C. T. Chao, "*MCNPX simulation of proton dose distribution in homogeneous and CT phantoms*". Radiat. Phys. Chem. 2014, 95:302-4.
9. G. Battistoni, S. Muraro, P. R. Sala, F. Cerutti, A. Ferrari, and S. Roesler, "*in Hadronic Shower Simulation Workshop*", edited by M. Albrow and R. Raja (American Institute of Physics, Batavia, 2006), Vol. 896, pp. 31–49.
10. L. S. Waters, J. Hendricks, and G. McKinney, "*Monte Carlo N-Particle Transport Code system for Multi-particle and High Energy Applications*". (Los Alamos, NM: Los Alamos National Laboratory, 2002).
11. S. Agostinelli, J. Allison, K. Amako, et al., "*Geant4-a simulation toolkit".* Nucl. Instrum. Meth. A, 2003, 506:250-303.
12. J. Apostolakis et al., "*Geometry and physics of the Geant4 toolkit for high and medium energy applications*". Radiat. Phys. Chem. 2009, **78**:859–873.
13. H Bethe, "*Zur theorie des durchgangs schneller korpuskularstrahlen durch Materie*". Ann. Phys., 1930, 5:324-400.
14. F Bloch,"*Zur bremsung rasch bewegter teilchen beim durchgang durch Materie*". Ann. Phys., 1933, 16:285-320.
15. U. Fano, "*Penetration of protons, alpha particles and mesons*". Annu. Rev. Nucl. Sci, 1963, 13:1-66.
16. W. D. Newhauser and R. Zhang, "*The physics of proton therapy*". Physics in Medicine and Biology, 2015, 60(8):R155.
17. K. Nakamura et al, "*Review of Particle Physics*". Phys. Rev. G, 37. Available at http://pdg.lbl.gov
18. V.L. Highland, "*Some practical remarks on multiple scattering*". Nucl. Instrum. Meth., 1975, 129:497.
19. G. Kraft, "*Tumor therapy with heavy charged particles*". Prog. Part. Nucl. Phys., 200, 45:S473–S544.
20. B. Gottschalk, A.M. Koehler, R.J. Schneider, J.M. Sisterson, and M.S. Wagner, "*Multiple Coulomb scattering of 160 MeV protons*". Nucl Instrum Meth B, 1993, 74(4):467–490.
21. J. J. Bevelacqua, "*Systematics of heavy ion radiotherapy*". Radiation Protection managment, 2005, 22:4-13.
22. Physics Reference Manual, Version: geant4 10.0 (6 December 2013).
23. ROOT European Centre for Nuclear Research (CERN] available at http://root.cer..ch
24. R. Brun, F. Rademakers, "*ROOT – An object oriented data analysis framework*", *Nucl. Instr. Meth. Phys. Res*., **A389**[1-2], 81-86 (1997).
25. E. Pedroni , S. Scheib , T. Böringer, A. Coray, M. Grossman, S. Lin and A. Lomax, "*Experimental characterization and physical modeling of the dose distribution of scanned proton pencil beams*". Phys. Med. Biol., 2005, 50:541–561.
26. U. Schneider, S. Agosteo, E. Pedroni., *et al*., "*Secondary neutron dose during proton therapy using spot scanning*". Int. J. Radiat Oncol. Biol. Phys., 2002, 53:244–251.
27. E. J. Hall, "*Radiobiology for the radiologist*". fifth edn. Lippincot, Williams and Wilkins, Philadelphia (2000)
28. E. J. Hall, "*Intensity–modulated radiation therapy, protons, and the risk of second cancers*". Int. J. Radiat. Oncol. Biol. Phys. 2006, 65:1–7.
29. G. Coutrakon, *et al* "*Microdosimetry spectra of the Loma Linda proton beam and relative biological effectiveness comparisons*". *Med. Phys.* 1997, 24:1499.
30. M. J. Berger, J. S. Coursey, M. A. Zucker, and J. Chang, "*estar, pstar, and astar: Computer Programs for Calculating Stopping-Power and Range Tables for Electrons, Protons, and Helium Ions*" (version 1.2.3). National Institute of Standards and Technology, Gaithersburg, MD, 2005, available athttp://physics.nist.gov/Star .